Thermodynamics and Structures of Amide Phospholipid Monolayers

Xiuhong Zhai,[†,‡] Gerald Brezesinski,*[,‡] Helmuth Möhwald,[‡] and Junbai Li*[,†]

International Joint Lab, Key Lab of Colloid and Interface Science, The Center for Molecular Science, Institute of Chemistry, Chinese Academy of Sciences, Zhong Guan Cun, Beijing 100080, China, and Max Planck Institute of Colloids and Interfaces, Am Muehlenberg 1, D-14476 Golm/Potsdam, Germany

Received: June 23, 2004

Monolayers of newly synthesized amide phospholipids, 1-*O*-hexadecyl-2-*N*-palmitoyl-2-amino-2-deoxy-*sn*-glycero-3-phosphocholine (L-ether-amide-PC) and 1-palmitoyl-2-*N*-palmitoyl-2-amino-2-deoxy-*sn*-glycero-3-phosphocholine (L-ester-amide-PC) were investigated at the air/subphase interface by Brewster angle microscopy combined with a conventional LB trough and Grazing incidence X-ray diffraction (GIXD). Both systems investigated exhibit two-dimensional domains with characteristic shape in the coexistence region between liquid-expanded (LE) and liquid-condensed (LC) phases. Especially L-ether-amide-PC shows highly chiral domains depending on temperature. The largest chiral domains (400 μm) growing in a clockwise direction are obtained at 25 °C. Such large domains have rarely been observed for phospholipids before. Thermodynamic data derived from $\pi-A$ isotherms provide information about critical temperature (T_c) and phase transition enthalpy (ΔH) for both amide phospholipids. The amide group leads to pronounced differences in the thermodynamic parameters compared with DPPC. The two-dimensional structures of the monolayers were investigated by GIXD. The results show that both amide phospholipids exhibit chiral in-plane structures. In the case of L-ether-amide-PC, the tilt angle of the aliphatic chains decreases only slightly with increasing pressure. On the contrary, the tilt angle of the aliphatic chains of L-ester-amide-PC shows strong dependence on surface pressure similar to DPPC. Possible hydrogen bonds involving the amide group seem to enhance the chiral interaction and play therefore a key role in the formation of extremely large chiral domains. The affects of substitution in the *sn*-1 position on structure formation are discussed in detail.

Introduction

Sn-2 amide analogues of phospholipids are known as strong inhibitors of the secretory phospholipase A_2 when the alkyl chain at the sn-1 position of the glycerol backbone is connected by an ester, ether, or thioether bond.[1−4] Phospholipase A_2 (PLA_2) is a calcium-dependent enzyme,[5−7] which hydrolyzes stereospecifically the ester bond at the sn-2 position of the glycerol backbone of phospholipids to release fatty acids and lysophospholipids,[8] preferentially if the phospholipids are in an aggregated state.[9,10] PLA_2 is widespread in bacteria, snake and bee venoms, mammalian cells, and secretions.[11,12] Amide phospholipids, which cannot be hydrolyzed, are valuable tools since they allow the study of interactions with PLA_2 without disturbing effects due to hydrolysis products. We have used newly synthesized enantiomeric sn-2 amide analogues, L-ether-amide-PC and L-ester-amide-PC, to study the interactions with PLA_2. Both molecules have a chiral center at the sn-2 position of the glycerol backbone and were therefore additionally interesting for the study of formation of chiral structures in monolayers at the air/water interface. The main question of this study is how the chemical structure of amphiphiles influences microscopic and molecular structures of a monolayer.[13−16]

The investigation of thermodynamic properties, molecular structures, and specific interactions with PLA_2 can also help to better understand the influence of particular structural elements on the adsorption of PLA_2 at the membrane surface as well as on the inhibition of the hydrolysis reaction.[17] Brewster angle microscopy opens a new prospect for the direct visualization of domain shapes in Langmuir monolayers.[18−20] It allows characterizing the long-range orientational order in the assembly of a phospholipid monolayer owing to the optical anisotropy induced by tilted aliphatic chains.[21−23] In the present work, this method is used to visualize the morphologies of L-ether-amide-PC and L-ester-amide-PC monolayers in the temperature range from 10 to 35 °C. Apart from observation on the micrometer scale, grazing incidence X-ray diffraction (GIXD) measurements as a function of surface pressure have been performed at 20 °C to evaluate the monolayers structure on the Å scale.

Experimental Section

Materials. 1-*O*-Hexadecyl-2-*N*-palmitoyl-2-amino-2-deoxy-*sn-glycero*-3-phosphocholine (L-ether-amide-PC) and 1-palmitoyl-2-*N*-palmitoyl-2-amino-2-deoxy-*sn-glycero*-3-phosphocholine (L-ester-amide-PC) were synthesized based on the procedures described previously[17,24] and have been characterized by NMR. The relevant chemical structures are shown in Scheme 1. L-Dipalmitoylphosphatidylcholine (L-DPPC) was purchased from Sigma and used without further purification. Chloroform of 99%+ purity was purchased from ACROS. The water in all experiments was purified by a Milli-Q system.

Film Balance Measurements. The temperature-dependent pressure−area ($\pi-A$) isotherms were measured on a Langmuir trough (R&K, Potsdam, Germany) equipped with a Wilhelmy-type pressure measuring system. The surface pressure was

* Address correspondence to these authors. G.B.: phone (+49) 331-5679234, fax (+49) 331-5679202, e-mail brezesinski@mpikg-golm.mpg.de. J.L.: phone (+86) 10-82614087, fax (+86) 10-82612629, e-mail jbli@iccas.ac.cn.

† Chinese Academy of Sciences.

‡ Max Planck Institute of Colloids and Interfaces.

10.1021/jp047260d CCC: $27.50
Published on Web 08/06/2004

SCHEME 1: The Chemical Structures of (a) 1-O-hexadecyl-2-N-palmitoyl-2-amino-2-deoxy-sn-glycero-3-phosphocholine (L-Ether-amide-PC) and (b) 1-Palmitoyl-2-*N*-palmitoyl-2-amino-2-deoxy-*sn*-glycero-3-phosphocholine (L-ester-amide-PC)

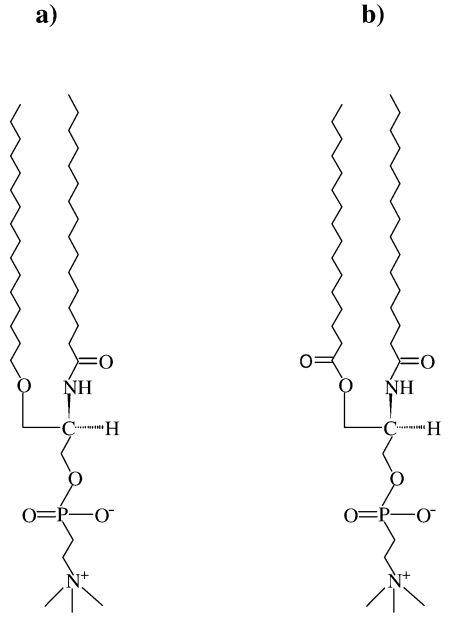

measured within 0.1 mN/m. The L-ether-amide-PC and L-ester-amide-PC monolayers were prepared from 1 mM phospholipid/chloroform solutions on a buffer subphase at pH 8.9 containing 150 mM NaCl, 5 mM $CaCl_2$, and 10 mM Tris (optimal conditions for PLA_2). In all experiments, the compression rate was 2 (Å^2 molecule^{-1})/min.

Brewster Angle Microscopy (BAM). A Brewster angle microscope (BAM-2) from NFT (Göttingen, Germany) mounted on the film balance was used for observation of the monolayer in the micrometer range. The microscope is sensitive to changes of the refractive index resulting from differences in thickness, density, and molecular orientation. The resolution is about 2 μm. Optical anisotropy caused by different molecular orientation in the monolayer is detected by an analyzer in the reflected beam path. The reflected light passes through a lens to a CCD (charge coupled device) camera, and the resulting video signal is fed to a video system. The BAM images are treated with an image processing software from Compic (Germany) to correct the distortion resulting from the observation at the Brewster angle. Changes in surface pressure as well as of monolayer morphology were simultaneously recorded.

Synchrotron X-ray Diffraction. Grazing incidence X-ray diffraction (GIXD) experiments were performed with the liquid-surface diffractometer on the undulator beamline BW1 at HASYLAB, DESY, Hamburg, Germany. A monochromatic synchrotron beam strikes the air/water interface at a grazing incidence angle $\alpha_i = 0.85\alpha_c$, where α_c is the critical angle for total external reflection. The diffracted intensity is detected by a linear position-sensitive detector (PSD) (OED-100-M, Braun, Garching, Germany) as a function of the vertical scattering angle α_f. A Soller collimator is located in front of the PSD and provides the resolution for the horizontal scattering angle $2\theta_{xy}$. The horizontal (in-plane) component of the scattering vector **Q** is given by $Q_{xy} \approx (4\pi/\lambda)\sin(\theta_{xy})$ and the vertical (out-of-plane) component is given by $Q_z \approx (2\pi/\lambda)\sin(\alpha_f)$, where λ is the X-ray wavelength.[25−27] The diffracted intensities were corrected for polarization, effective area, and Lorentz factor. Model peaks taken to be Lorentzian in the in-plane direction and Gaussian in the out-of-plane direction were fitted to the corrected intensities. From the peak positions we can obtain the lattice parameters and the tilt angle *t*. The cross-sectional area of the chains is given by $A_0 = A_{xy}\cos(t)$, where A_{xy} is the area per acyl chain in the water plane.

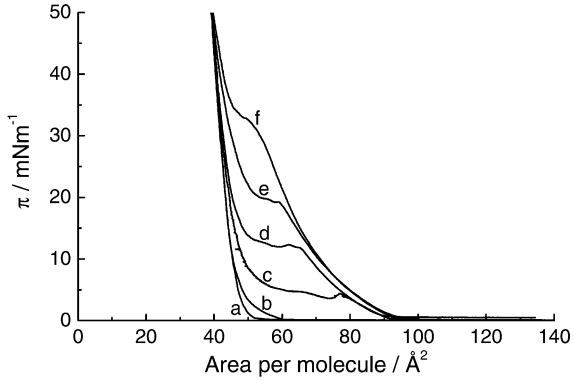

Figure 1. Lateral pressure (π) as a function of molecular area (*A*) of L-ether-amide-PC monolayers at different temperatures: (a) 10, (b) 15, (c) 20, (d) 25, (e) 30, and (f) 35 °C.

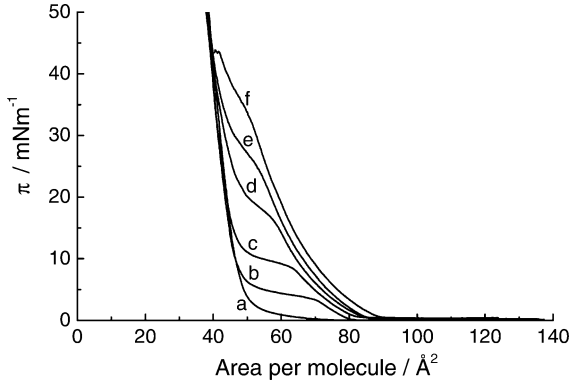

Figure 2. Lateral pressure (π) as a function of molecular area (*A*) of L-ester-amide-PC monolayers at different temperatures: (a) 10, (b) 15, (c) 20, (d) 25, (e) 30, and (f) 35 °C.

Results and Discussion

Thermodynamics and Morphology of the Amide Phospholipid Monolayers. L-Ether-amide-PC is a mixed linked phospholipid: the linkage group at the sn-1 position of the glycerol backbone is an ether group and the one at the sn-2 position is an amide group. Compared with DPPC, L-ester-amide-PC has the same linkage group in the sn-1 position but an amide group in the sn-2 position. In contrast to the diester lipid DPPC, the amide group allows the formation of hydrogen bondings.[28−30] Therefore, it can be expected that aggregation behavior in monolayers at the air/water interface should be different compared with that of diester or diether PC lipids. First of all, we have performed isotherm measurements of the surface pressure π as a function of molecular area *A* at different temperatures (10−35 °C). Figures 1 and 2 show the isotherms of L-ether-amide-PC and L-ester-amide-PC, respectively. The plateau region corresponding to the coexistence of liquid-expanded (LE) and liquid-condensed (LC) phases shifts to higher surface pressures with increasing temperature for both amide phospholipids. The transition pressure, π_t, seems to be a linear function of the temperature (Figure 3a). Usually, deviations from such a linear behavior are observed close to T_0, the temperature below which no LE phase exists. The temperature coefficients $d\pi/dT$ amount to 1.64 for L-ether-amide-PC and 1.40 for L-ester-amide-PC. For comparison, the temperature coefficient of DPPC

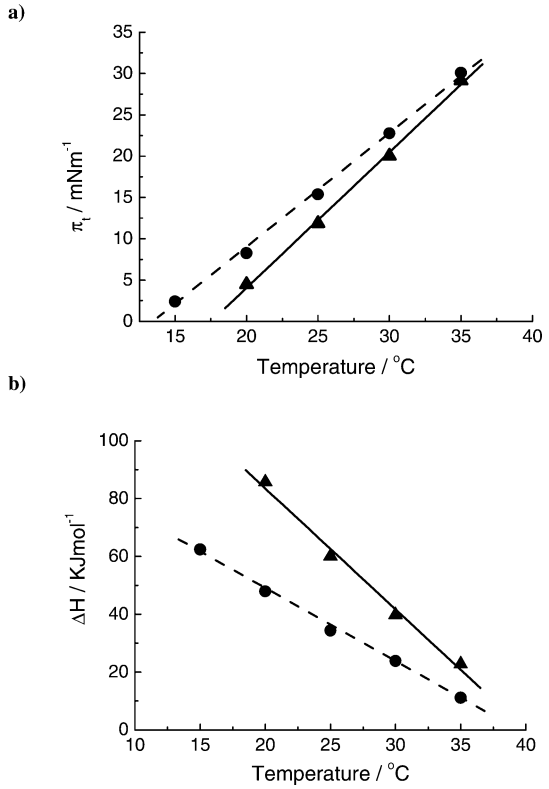

Figure 3. (a) Lateral pressure (π_t) of the main phase transition (LE-LC) of L-ether-amide-PC (▲) and L-ester-amide-PC (●) monolayers versus temperature. (b) Transition enthalpies (ΔH) as function of temperature for L-ether-amide-PC (▲) and L-ester-amide-PC (●) monolayers. ΔH was calculated by using a modified Clausius−Clapeyron equation.

is 1.38.[31] Linear extrapolations yield $T_0 = 17.5$ °C for the L-ether-amide-PC and $T_0 = 13.8$ °C for the L-ester-amide-PC.

The phase transition enthalpy ΔH gives additional information about the effect of chemical groups on the LE/LC phase transition.[32] From the area change $\Delta A = A_E - A_C$ it is possible to calculate the transition enthalpy by using a modified Clausius−Clapeyron equation $d\pi/dT = \Delta H/(T(A_E - A_C))$, where T is the subphase temperature, A_E is the molecule area in the LE phase at the plateau onset, A_C is the molecular area in the LC phase extrapolated to the transition pressure, and $d\pi/dT$ is the temperature coefficient of the transition pressure. ΔH as a function of temperature is plotted in Figure 3b. Linear extrapolations toward $\Delta H = 0$ yield the critical temperatures T_c of about 40 °C for the *T*-ether-amide-PC and 39.1 °C for the *T*-ester-amide-PC. T_c is that temperature above which a condensed monolayer phase cannot be achieved by compression. Comparison with DPPC shows that the observed T_c values are similar to that of DPPC. However, in the case of DPPC T_c equals T_m (main transition temperature from gel to liquid-crystalline phases in aqueous dispersions) indicating similar packing properties in mono- and bilayers. For *T*-ester-amide-PC, the T_c value (39.1 °C) was also similar to the T_m value (39.7 °C). However, in the case of *T*-ether-amide-PC, T_m (47 °C)[24] is considerably higher than T_c indicating distinct differences in packing properties between mono- and bilayers.

Figure 4 presents BAM images of *T*-ether-amide-PC at different temperatures in the coexistence region. Domains typical of the first-order phase transition between LE and LC can be seen even at 15 °C. This means that there must be a plateau region at a very low surface pressure, which cannot be seen in the isotherm. Below 15 °C, the LE/LC coexistence region is not observed. The BAM results are in perfect agreement with

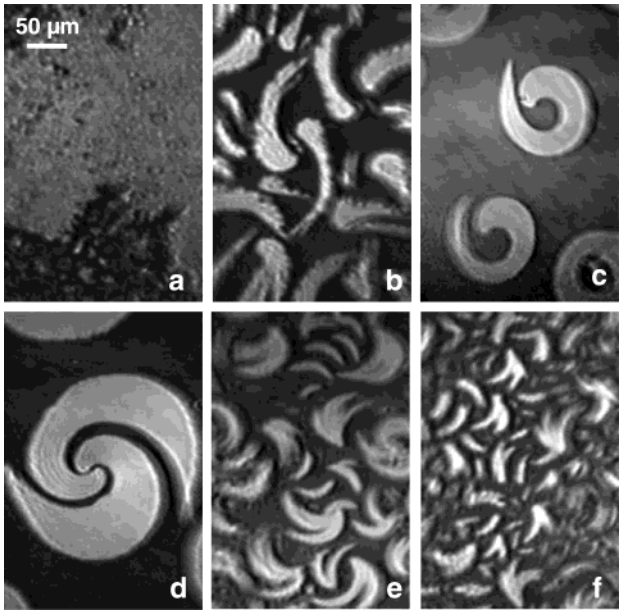

Figure 4. BAM images of L-ether-amide-PC monolayers at (a) 10, (b) 15, (c) 20, (d) 25, (e) 30,and (f) 35 °C. The images were taken in the coexistence regions.

our isotherm measurements. Domains appear only above the phase transition pressure. There are no regular domains at 10 °C where the condensed phase is produced during the spreading process. At zero pressure, islands of a condensed phase coexist with a gaseous phase (Figure 4a). At 15 °C, chiral domains are observed at $\pi = 0.5$ mN/m (Figure 4b). The expected two-phase coexistence region cannot be well recognized in the isotherm. However, the pressure increases already at molecular areas of approximately 60 Å^2 indicating that there could be a plateau region at very low pressure.

At 20 °C, the pressure−area isotherm shows a clear first-order phase transition from a liquid expanded to a condensed state. Clockwise chiral domains appeared in the entire coexistence region of LE and LC phases (Figure 4c). The transition is connected with an overcompression of the liquid-expanded phase (thermodynamic instability). At lateral pressures above the equilibrium transition pressure the first nuclei of a condensed phase are formed. On further compression, the lateral pressure drops to the equilibrium value and growth of chiral domains can be observed. The compression leads to a dramatic increase of the domain size, and the number of domains is almost unchanged. If the domains grow to a certain size they come together and start to fuse in the condensed-phase region.[33] Chiral domains formed at the air/water interface must have a long-range molecular orientational order. This orientation must play a key role in forming the chiral structure and hence induces the domain growth up to 300 μm, which was rarely observed for phospholipids before. The stability of the chiral domains is remarkably high. Figure 4d displays typical domains appearing at 25 °C in the transition region. The growth direction of symmetrically spiral domains is clockwise. During the growth of the chiral domains, they coalesce and fuse to form huge domains. The largest chiral domains are observed with a diameter of approximately 400 μm.[33]

However, the continuous increase of temperature does not lead to further growth of the chiral domains. The domains possess a similar spiral structure at 30 °C but with a smaller size (Figure 4e). At 35 °C, the domains are much smaller and exhibit several arms (Figure 4f). This means that increasing temperature diminishes the influence of the chiral center on the

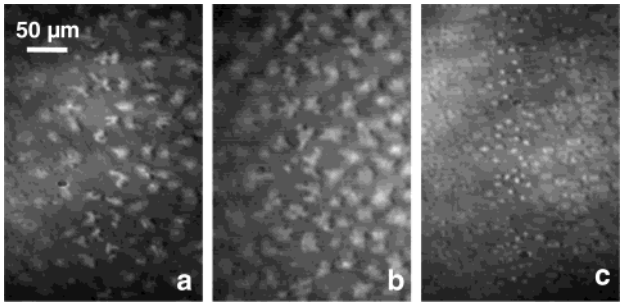

Figure 5. BAM images of L-ester-amide-PC monolayers at (a) 15, (b) 20,and (c) 25 °C. The images were taken in coexistence regions.

two-dimensional arrangement in molecular aggregates. A higher compression rate also reduces the domain size.

The formation of chiral domains depends on the experimental conditions such as temperature and compression rate. These conditions influence, for instance, the anisotropy of the line tension. Furthermore the growth kinetics can be influenced. The linkage group between hydrophobic chains and the headgroup of the amide phospholipid obviously plays a key role. The amide group can form hydrogen bonds enhancing the effect of chirality. On the other hand, increasing temperature weakens these interactions and consequently influences the growth kinetics. At low temperature, the nucleation process is dominating and the domains do not grow to a very large size. At higher temperature, the growth rate is dominating. Additionally, chiral interactions as well as hydrogen bonds are affected by the temperature leading again to smaller domains at higher temperatures.[34]

For comparison, Figure 5 shows the BAM images of the L-ester-amide-PC in the LE/LC coexistence region at 15, 20, and 25 °C. Anisotropic domains with an irregular shape appear above the phase transition pressure. There are no pronounced chiral domains at all temperatures investigated as in the case of the L-ether-amide-PC. At 20 °C, the size of the domains (Figure 5b) is similar to that of L-DPPC. However, the corresponding phase transition pressure is higher than that for L-DPPC. Above 25 °C, the size of the domains is also drastically decreased and only small circular domains can be seen instead of irregular shaped ones (Figure 5c).

Comparing the chemical structures, one can see that the linkage group in the sn-1 position plays the key role. Molecular and chiral interactions are changed. These changes influence the growth kinetics. The following GIXD investigations could provide further information on the influence of chirality and molecular interactions on the structure formation.

Lattice Structure Analysis by GIXD. Influence of chirality on the thermodynamic behavior and the morphology in 2D structures was also found for other amphiphilic monolayers including phospholipids.[35] In general, it is believed that intermolecular interactions should play a key role. To better understand the influence of chirality on the phase behavior of the L-ether-amide-PC and L-ester-amide-PC, the monolayers were examined by grazing incidence X-ray diffraction (GIXD) to determine the in-plane structures on the angstrom scale. Figure 6 shows selected contour plots of the corrected X-ray intensities as a function of the in-plane scattering vector component Q_{xy} and the out-of-plane scattering vector component Q_z at 30 mN/m for both amide phospholipids in comparison with L-DPPC at the same surface pressure. For L-ether-amide-PC, the monolayer exhibits three low-order diffraction peaks at all pressures investigated. Such an intensity profile is characteristic for an oblique (chiral) chain lattice. The maxima

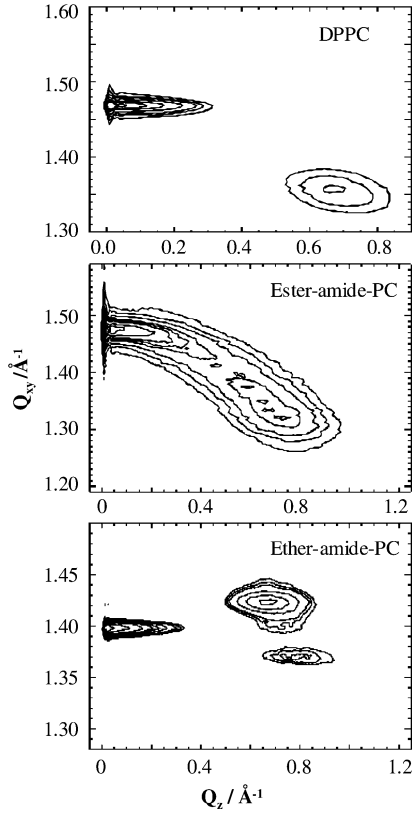

Figure 6. Contour plots of corrected X-ray intensities as a function of in-plane scattering vector component Q_{xy} and out-of-plane scattering vector component Q_z of L-ether-amide-PC, L-ester-amide-PC, and L-DPPC monolayers (indicated) on water at 20 °C and 30 mN/m.

of the Bragg rods are above the horizon, thus the chains are tilted from the perpendicular orientation to the surface in a nonsymmetry direction. L-Ester-amide-PC also shows three Bragg peaks of an oblique chain lattice; however, the scattered intensity is more distributed on an arc indicating that in this case the molecules are not tilted in a well-defined tilt direction. The phase transition from liquid expanded to condensed is driven by aliphatic tail ordering and specific interactions between the headgroups. Chiral interactions usually have a rather weak influence on the structure formation in comparison with other interactions between amphiphilic molecules since the chiral center is only a small part of the molecule. Usually, chirality of phospholipids results therefore in oblique unit cells quite close to the rectangular ones, as observed for L-DPPC. Stronger effects of chiral interactions can be expected close to phase transitions where other interactions compensate, or if a directed interaction enhances the chiral interactions. Therefore, the amide linkage group in the sn-2 position seems to be the enhancing factor leading to more pronounced chiral lattices. On the other hand, this enhancing effect is more pronounced for the ether-PC compared with the ester-PC. Obviously, the ester group in the sn-1 position reduces the influence of the amide group.

The corresponding structural parameters for L-ether-amide-PC and L-ester-amide-PC are shown in Tables 1 and 2, respectively. For L-ether-amide-PC, the cross-sectional area of a chain amounts to 19.8−19.9 Å^2. This value is slightly smaller than that of L-DPPC (20.1−20.2 Å^2) indicating a slightly tighter packing of the chains.[36] For the L-ester-amide-PC, the cross-sectional area of the chain (20.3−20.5 Å^2) is larger than that of L-DPPC. Compared with the L-ether-amide-PC, the packing is disturbed due to the ester linkage group in the sn-1 position. This looser packing is connected with the formation of small

TABLE 1: Bragg Peak (Q_{xy}) and Bragg Rod (Q_z) Maxima, Lattice Distortion (d), Tilt Angle (t), and Cross-Sectional Area (A_0) at 20 °C and Different Lateral Pressures of L-Ether-amide-PC

	π (mN/m)			
	8.1	20	30	40.2
peak1 Q_{xy}/Q_z[a]	1.346/0.859	1.361/0.818	1.370/0.795	1.384/0.749
peak 2 Q_{xy}/Q_z[a]	1.391/0.171	1.395/0.129	1.397/0.120	1.400/0.080
peak 3 Q_{xy}/Q_z[a]	1.416/0.688	1.421/0.679	1.424/0.675	1.428/0.669
distortion	0.05894680	0.04982122	0.04462371	0.03670296
tilt angle[b]	33.7	32.5	31.7	30.4
A_0[c]	19.8	19.8	19.9	19.9

[a] In Å^{-1}. [b] In deg. [c] In Å^2.

TABLE 2: Bragg Peak (Q_{xy}) and Bragg Rod (Q_z) Maxima, Lattice Distortion (d), Tilt Angle (t), and Cross-Sectional Area (A_0) at 20 °C and Different Lateral Pressures of L-Ester-amide-PC

	π (mN/m)		
	19.7	29.5	39.7
peak 1 Q_{xy}/Q_z[a]	1.308/0.735	1.324/0.717	1.378/0.610
peak 2 Q_{xy}/Q_z[a]	1.390/0.601	1.403/0.517	1.412/0.438
peak 3 Q_{xy}/Q_z[a]	1.467/0.134	1.466/0.200	1.474/0.172
distortion	0.1318755	0.1170386	0.07940509
tilt angle[b]	31.1	29.4	24.7
A_0[c]	20.4	20.4	20.5

[a] In Å^{-1}. [b] In deg. [c] In Å^2.

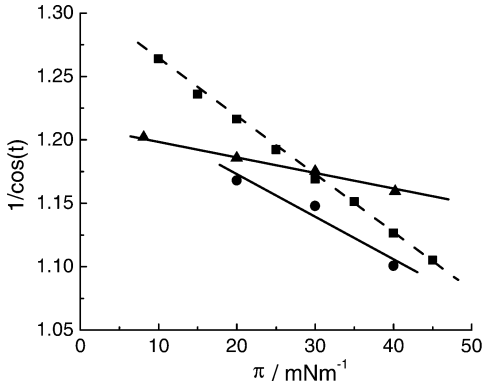

Figure 7. Plots of 1/cos(t) versus the surface pressure for L-ether-amide-PC (▲), L-ester-amide-PC (●), and L-DPPC (■). Extrapolation to 1/cos(t) = 1 gives the theoretical pressure at which the tilt angle becomes zero: π_{tr} = 163.5 mN/m for L-ether-amide-PC, π_{tr} = 71.3 mN/m for L-ester-amide-PC, and π_{tr} = 68.3 mN/m for DPPC. The extrapolation to zero pressure yields the maximum tilt angles of t_{max} = 34.4° for L-ether-amide-PC, t_{max} = 36.3° for L-ester-amide-PC, and t_{max} = 40° for DPPC.

irregular domains. On the other hand, from the comparison of the tilt angle of the chains, one can see that the tilt angle is much less pressure dependent for L-ether-amide-PC compared with L-ester-PC and L-DPPC (Figure 7). Increasing the lateral pressure from 8 to 40 mN/m leads only to a tilt angle decrease from 34° to 30°, whereas in the case of DPPC the tilt angle decreases from 35° at 14 mN/m to 25° at 41 mN/m, and for L-ester-amide-PC the tilt angle decreased from 31° at 20 mN/m to 25° at 40 mN/m. The slopes of these curves show a pronounced similarity for L-ester-PC and L-DPPC, whereas L-ether-amide-PC behaves considerably different. This small pressure dependence of the tilt angle of L-ether-PC could be an additional support for the assumption of the formation of hydrogen bonds, which lead to a more fixed structure.

The lattice distortion d of the L-ether-amide-PC, L-ester-amide-PC, and L-DPPC versus sin^2t (t is the tilt angle of the aliphatic chains) is shown in Figure 8. The linear dependence

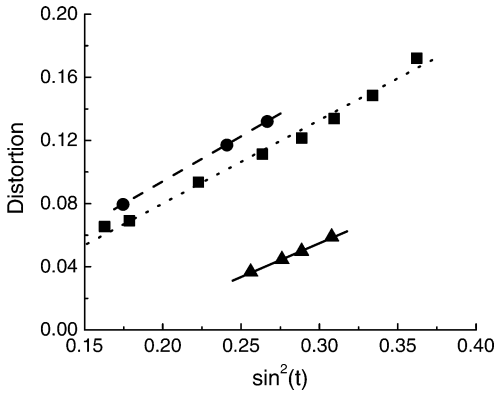

Figure 8. Lattice distortions of the L-ether-amide-PC (▲), L-ester-amide-PC (●), and L-DPPC (■) monolayers versus sin^2(t). The nonzero intercept d_0 indicates additional contributions to the lattice distortion due to ordering of the zigzag planes of the chains. The $|d_0|$ values are 0.073 for L-ether-amide-PC, 0.020 for L-ester-amide-PC, and 0.022 for L-DPPC.

can be expected from a Landau theory.[34] One reason for the lattice distortion is the molecular tilt, but the nonzero intercept d_0 indicates additional contributions due to ordering of the zigzag planes of the chains (hindered rotation). The absolute values of d_0 are 0.073 for L-ether-amide-PC, 0.020 for L-ester-amide-PC, and 0.022 for L-DPPC. This indicates that the contribution of chain packing is very similar for L-ester-amide-PC and L-DPPC and very small, so that the main reason for the lattice distortion is the tilting of the molecules. However, the hindered rotation of L-ether-amide-PC is much more pronounced. One reasonable assumption for this effect could be again the formation of hydrogen bonds.

L-Ester-amide-PC and L-DPPC both have an ester bond in the sn-1 position but the linkage group in the sn-2 position is different (amide bond and ester bond, respectively). The substitution of an ester linkage group by the amide group caused changes in the domain morphology from roughly circular for L-DPPC[37] to an irregular shape for the L-ester-amide-PC. The tilt angles, cross-sectional areas of the chains, and lattice distortion are very similar, indicating a close relation between monolayer structure and domain morphology. The change of the linkage group in the sn-1 position of the amide lipids from ester to ether has a much bigger influence on the monolayer structure and domain morphology. The ether linkage leads to clearly chiral domain shapes and much larger domain sizes. The tilt angle is much less pressure dependent indicating that the structure is fixed by additional interactions. The cross-sectional area is smaller, and the chain packing is much tighter. This shows that the larger anisotropy of the lattice causes a larger anisotropy of the domain. The more pronounced chiral interactions in L-ether-amide-PC monolayers compared with L-ester-amide-PC monolayers must be due to tighter packing of the smaller ether group.

From the fwhm (full-width at half-maximum) of the Bragg peaks we can calculate the finite size L_{xy} of the 2D crystallites. A finite size of the crystalline domains gives rise to a broadening of the Bragg peaks. The fwhm of the Bragg peaks usually exceeds the instrumental resolution (0.008 Å^{-1}), only for L-ether-amide-PC resolution limited peaks that are observed at low lateral pressure. Fwhm of the L-ester-amide-PC peaks is in all cases much larger than that of L-ether-amide-PC peaks. The positional correlation of the chain lattice in different directions is different. In the case of L-ether-amide-PC, increasing the lateral pressure leads to a broadening of all peaks indicating that the correlation length of the lattice is decreasing on

compression. This shows that the lattice is better ordered at low pressure because of an optimization of forces between the molecules. Therefore, one might think that possible hydrogen bonds involving the amide groups may play an important role. These hydrogen bonds could also lead to a preferred growth direction of the domain and could be responsible for the very small change of the tilt angle and other lattice parameters during compression. Additionally, the hydrogen bonds could also enhance the chiral interaction and thus result in the very large chiral domains. The situation is different for the L-ester-amide-PC, where the fwhm of the two Bragg peaks at higher Q_z increases on compression and only that of the peak close to the horizon decreases. This different behavior again points at the above-discussed differences between the two amide-PCs due to a different ability to form hydrogen bonds.

Conclusion

Thermodynamic and textural characterizations of the amide phospholipids monolayers have been performed by measurements of $\pi-A$ isotherms and BAM at different temperatures between 10 and 35 °C. The surface pressure of the first-order phase transition increases linearly with increasing temperature. For L-ether-amide-PC, the domains formed in the coexistence region are highly chiral and grow in a clockwise direction. The shape and size are strongly temperature dependent. The largest domains (up to 400 μm) have been observed at 25 °C. In the case of L-ester-amide-PC, irregularly shaped domains can be observed in the LE/LC coexistence region with a similar size as seen for L-DPPC. The possibility of intermolecular hydrogen bond formation could play the key role in the domains growth. The GIXD results show that the in-plane lattice is chiral (oblique) for both amide phospholipids. However, L-ether-amide-PC exhibits much larger lattice anisotropy. The tilt angle of the chain does not change significantly with increasing pressure for L-ether-amide-PC. The pressure dependence of the tilt angle is unusually small. On the contrary, L-ester-amide-PC shows a pressure dependence of the tilt angle, which is very similar to that of L-DPPC. We assume that in the case of L-ether-amide-PC the influence of the chiral center on the lattice structure and domain shape is enhanced by hydrogen bonds between the amide groups. Such hydrogen bonds are suppressed by the ester linkage group in the sn-1 position in the case of L-ester-amide-PC. The lattice distortion from hexagonal is much larger for L-ether-amide-PC compared with L-ester-amide-PC indicating again that the chiral interactions are enhanced possibly by hydrogen bonds. Obviously, the formation of hydrogen bonds is strongly influenced by the type of linkage group in the sn-1 position for both amide phospholipids. The formation of highly chiral domains is well correlated with the degree of chirality of the chain lattice.

Acknowledgment. The authors wish to acknowledge Dr. Bernd Rattay and Markus Bartel (University of Halle/S., Germany) for synthesizing the amide phospholipids. We thank the Chinese Academy of Sciences as well as the collaboration project of the German Max Planck Society. We also thank HASYLAB (DESY, Hamburg, Germany) for providing beamtime and Kristian Kjaer for his valuable help at the beamline BW1.

References and Notes

(1) Bonsen, P. P. M.; de Haas, G. H.; Pieterson, W. A.; van Deenen, L. L. M. *Biochim. Biophys. Acta* **1972**, *270*, 364−382.
(2) Davidson, F. F.; Hajdu, J.; Dennis, E. A. *Biochem. Biophys. Res. Commun.* **1986**, *137*, 587−592.
(3) de Haas, G. H.; Dijkman, R.; Ransac, S.; Verger, R. *Biochim. Biophys. Acta* **1990**, *1046*, 249−257.
(4) Yu, L.; Deems, R. A.; Hajdu, J.; Dennis, E. A. *J. Biol. Chem.* **1990**, *265*, 2657−2664.
(5) Janda, J. M.; Bottone, E. J. *J. Clinic. Microbiol.* **1981**, *14*, 55−60.
(6) Gelb, M. H.; Jain, M. K.; Berg, O. *Bioorg. Med. Chem. Lett.* **1992**, *2*, 1335−1342.
(7) Verger, R.; de Haas, G. H. *Chem. Phys. Lipids* **1973**, *10*, 127−136.
(8) Dahmen-Levison, U.; Brezesinski, G.; Möhwald, H. *Prog. Colloid Polym. Sci.* **1998**, *110*, 269−274.
(9) Chang, J.; Musser, J. H.; McGregor, H. *Biochem. Pharmacol.* **1987**, *36*, 2429−2436.
(10) Li, J. B.; Chen, Z. J.; Wang, X. L.; Brezesinski, G.; Möhwald, H. *Angew. Chem., Int. Ed.* **2000**, *39*, 3059−3062.
(11) van den Bosch, K. *Biophys. Acta* **1980**, *604*, 191−246.
(12) Béréziat, G.; Etienne, J.; Kokkinidis, M.; Oliver, J. L.; Pernas, P. *J. Lipid Mediators* **1990**, *2*, 159−172.
(13) Möhwald, H. *Thin Solid Film* **1988**, *159*, 1−15.
(14) Knobler, C. M. *Adv. Chem. Phys.* **1990**, *77*, 397.
(15) Gehlert, U.; Vollhardt, D. *Prog. Colloid Polym. Sci.* **1994**, *97*, 302.
(16) Weidemann, G.; Vollhardt, D. *Biophys. J.* **1996**, *70*, 2758.
(17) Bartel, M.; Rattay, B.; Nuhn, P. *Chem. Phys. Lipids* **2000**, *107*, 121−129.
(18) Hénon, S.; Meunier, J. *J. Rev. Sci. Instrum.* **1991**, *62*, 936−939.
(19) Hönig, D.; Möbius, D. *J. Phys. Chem.* **1991**, *95*, 4590−4592.
(20) Melzer, V.; Vollhardt, D. *Phys. Rev. Lett.* **1996**, *76*, 3770−3773.
(21) Fischer, T. M.; Bruinsma, R. F.; Knobler, C. M. *Phys. Rev.* **1994**, *E 50*, 413−428.
(22) Weidemann, G.; Brezesinski, G.; Vollhardt, D.; DeWolf, D.; Möhwald, H. *Langmuir* **1999**, *15*, 2901−2910.
(23) Knobler, C. M.; Schwartz, D. K. *Curr. Opin. Colloid Interface Sci.* **1999**, *4*, 46−51.
(24) Zhai, X. H.; Bartel, M.; Brezesinski, G.; Rattay, B.; Möhwald, H.; Li, J. B. *Chem. Phys. Lipids* **2004**, submitted for publication.
(25) Kjaer, K. *Physica B* **1994**, *198*, 100−109.
(26) Als-Nielsen, J.; Jacquemain, D.; Kjaer, K.; Lahav, M.; Leveiller, F.; Leiserowitz, L. *Phys. Rep.* **1994**, *246*, 251−313.
(27) Rietz, R.; Rettig, W.; Brezesinski, G.; Bouwman, W. G.; Kjaer, K.; Möhwald, H. *Thin Solid Film* **1996**, *284*, 211−215.
(28) Wolf, S. G.; Leiserowitz, L.; Lahav, M.; Deutsch, M.; Kjaer, K.; Als-Nielsen, J. *Nature* **1987**, *328*, 63−66.
(29) Parazak, D. P.; Uang, J.; Turner, B.; Stine, K. J. *Langmuir* **1994**, *10*, 3787−3793.
(30) Vollhardt, D.; Gutberlet, T.; Emrich, G.; Fuhrhop, J.-H. *Langmuir* **1995**, *11*, 2661−2668.
(31) Yu, Z.-W.; Jin, J.; Gao, Y. *Langmuir* **2002**, *18*, 4530−4531.
(32) Rodriguez Patino, J. M.; Ruíz Domínguez, M. *Colloids Surf. A* **1996**, *114*, 287−296.
(33) Zhai, X. H.; He, Q.; Li, J. B.; Brezesinski, G.; Möhwald, H. *ChemPhysChem* **2003**, *4*, 1355−1358.
(34) Kaganer, V. M.; Möhwald, H.; Dutta, P. *Rev. Mod. Phys.* **1999**, 71 (3), 779−819.
(35) Vollhardt, D.; Gehlert, U. *J. Phys. Chem. B* **2002**, *106*, 4419−4423.
(36) Brezesinski, G.; Dietrich, A.; Struth, B.; Böhm, C.; Bouwman, W. G.; Kjaer, K.; Möhwald, H. *Chem. Phys. Lipids* **1995**, *76*, 145−157.
(37) Zhai, X. H.; Li, J. B.; Brezesinski, G.; He, Q.; Möhwald, H.; Lai, L. H.; Liu, Y.; Liu, L.; Gao, Y. *ChemBioChem* **2003**, *4*, 299−305.